J. Fluid Mech. (2007), *vol.* 576, *pp.* 445–456.
doi:10.1017/S0022112007004673 Printed in the United Kingdom

Double-diffusive instabilities of autocatalytic chemical fronts

J. D'HERNONCOURT[1], A. DE WIT[1] AND A. ZEBIB[2]

[1]Nonlinear Physical Chemistry Unit and Center for Nonlinear Phenomena and Complex Systems, CP 231, Université Libre de Bruxelles, 1050 Brussels, Belgium

[2]Mechanical and Aerospace Engineering, Rutgers University, Piscataway, NJ 08854-8058, USA
jdhernon@ulb.ac.be; adewit@ulb.ac.be; zebib@rutgers.edu

(Received 8 May 2006 and in revised form 30 October 2006)

Convective instabilities of an autocatalytic propagating chemical front in a porous medium are studied. The front creates temperature and concentration gradients which then generate a density gradient. If the front propagates in the direction of the gravity field, adverse density stratification can lead to Rayleigh–Taylor or Rayleigh–Bénard instabilities. Differential diffusivity of mass and heat can also destabilize the front because of the double-diffusive phenomena. We compare the stability boundaries for the classical hydrodynamic case of a bounded layer without reaction and for the chemical front in the parameter space spanned by the thermal and solutal Rayleigh numbers. We show that chemical reactions profoundly affect the stability boundaries compared to the non-reactive situation because of a delicate coupling between the double-diffusive and Rayleigh–Taylor mechanisms with localized density perturbations driven by the reaction. In the reactive case, a linear stability analysis identifies three distinct stationary branches of the instability. They bound a region of stability that shrinks with increasing Lewis number, in marked contrast to the classical double-diffusive layer. In particular a region of global and local stable stratification is susceptible to a counter-intuitive mechanism of convective instability driven by chemistry and double-diffusion. The other two regions display an additional contribution of localized Rayleigh–Taylor instabilities. Displaced-particle arguments are employed in support of and to elucidate the entire stability boundary.

1. Introduction

Convective motions can be driven in a quiescent fluid due to adverse density stratification in the gravitational field. In Rayleigh–Bénard convection the density field is driven by temperature gradients. The presence of an additional diffusing component can drive doubly-diffusive instabilities. In the classical case both temperature and concentration differences are imposed on the fluid by the environment as boundary conditions on surfaces located a finite distance apart. Using linear theory, Baines & Gill (1969) determined the stability boundaries. The case of a saturated porous layer was treated by Nield (1968). More detail is given in the books by Turner (1973) and Nield & Bejan (1992). When both thermal R_T and solutal R_c Rayleigh numbers are positive the instability is in the direct mode, while stability is obtained when both are negative. The double-diffusive mechanisms operate when they are of different signs. Direct double-diffusive fingering modes are observed when the Rayleigh number of the slower diffusing component (usually, and here assumed, the concentration) $R_c > 0$

and $R_T < 0$, even in a region of stable stratification. Oscillatory double-diffusive modes are triggered when $R_T > 0$ and $R_c < 0$ when the system is unstably stratified.

Several applications, such as reactive petroleum extraction, separation techniques in chromatographic columns and geological flows to name a few, may feature flow instabilities of reactive systems in porous media. In this context, it is of interest to analyse the influence of chemical reactions on this general picture of buoyancy-driven hydrodynamic instabilities. Propagating reaction–diffusion chemical fronts provide a mechanism for creation of internal concentration and temperature gradients. Rayleigh–Taylor instabilities immediately set in as a fingering instability of the diffusive interface if the density stratification is unstable (see Pojman & Epstein 1998; De Wit 2004 and references therein). Double-diffusive instabilities driven by chemical fronts are also possible if molar volume changes and heat are generated simultaneously upon reaction (Pojman & Epstein 1990; Kalliadasis, Yang & De Wit 2004). Propagating chemical fronts provide a simple model system in which to study the changes in hydrodynamic stability induced by the chemical reactions.

In the present paper, we study theoretically all possible buoyancy-driven instabilities of such chemical fronts travelling in porous media, focusing on the way chemical reactions change the classical stability boundaries of the pure Rayleigh–Bénard, Rayleigh–Taylor and double-diffusive instabilities. We show that chemistry significantly affects the stability domains and that the classical intuitive stability picture of stratified fluids in the gravity field sketched at the beginning of the introduction becomes more complicated in reactive fluids. To demonstrate this, we employ scales that cast the problem in terms of the usual Rayleigh numbers and compute linear stability boundaries in the (R_T, R_c)-plane for different Lewis numbers $Le > 1$. The region of convective instability in this case of intrinsic chemically generated density gradients in an infinite medium is much larger than its classical hydrodynamic counterpart. Wholly unexpected instabilities where the system is globally and locally stably stratified are uncovered. A chemically driven instability mechanism is identified and the stability boundaries explained by displaced particle arguments. Moreover all the instability branches are stationary.

The outline of this article is as follows: in § 2, we formulate the model, introduce the important dimensionless parameters of the problem and develop the linear stability analysis. In § 3, we present the stability boundaries of both the pure hydrodynamic and chemically driven cases before ending with a discussion.

2. Formulation

A two-dimensional porous medium of infinite extent is saturated with reactants. An autocatalytic chemical front is initiated to propagate upward with a velocity v^* (with the superscript * refering to a dimensional quantity). The motion is described in a coordinate system (z^*, y^*) moving with speed v^* and attached to the front (located at $z^* = 0$), with the gravity field aligned along $-z^*$ and y^* being the transverse direction. The reaction–diffusion convectionless state is characterized by the concentration c^* of the chemical species that determines the density. As the reaction is exothermic, the concentration front drives a temperature T^* front. We assume a linear density dependence on c^* and T^* according to

$$\rho^* = \rho_0\{1 - \alpha_c(c^* - c_0^*) - \alpha_T(T^* - T_0^*)\} \tag{2.1}$$

where ρ_0 is the mixture density at reference temperature T_0^* and at concentration $c^* = c_0^*$ with c_0^* being the initial concentration of c^* in the reagents. The concentration

and thermal expansion coefficients are respectively α_c and α_T. If both $\alpha_c > 0$ and $\alpha_T > 0$ then we have lighter products due to the contributions of both c^* and T^* and the upward propagating reaction–diffusion front is gravitationally unstable.

The reaction–diffusion base state determines the prevailing concentration gradient, rates of reaction and propagation speed and hence the important scales of the problem. These are $\Delta c = c_1^* - c_0^*$ for concentration $c^* - c_0^*$ with $c = c_1^*$ being the concentration of c in the products, $\phi\tau = \phi(\gamma \Delta c^2)^{-1}$ for time with γ the kinetic constant of the reaction and ϕ the porosity, $U = \sqrt{D_c/\tau}$ for velocity with D_c the medium diffusion coefficient, and $l = \sqrt{D_c \tau}$ for length. The temperature $T^* - T_0^*$ is scaled by $\Delta T = -\Delta H \Delta c/\rho_0 c_p$, where ΔH is the heat of reaction and is negative for the exothermic reaction considered here, and c_p is the constant pressure specific heat of the solvent. In a saturated porous medium the incompressible flow field is governed by the non-dimensional Darcy equations (Khan & Zebib 1981) written here with pressure incorporating the hydrostatic pressure and scaled by $\mu D_c/K$ where K and μ are the permeability and dynamic viscosity, respectively. Assuming ϕ is numerically equal to the ratio of the fluid to the medium heat capacities, the dimensionless equations of the problem take the form

$$\nabla \cdot \boldsymbol{u} = 0, \tag{2.2a}$$

$$\boldsymbol{u} = -\nabla p + (R_T T + R_c c)\boldsymbol{e}_z, \tag{2.2b}$$

$$\frac{\partial c}{\partial t} - v\frac{\partial c}{\partial z} + \boldsymbol{u} \cdot \nabla c = \nabla^2 c + F(c), \tag{2.2c}$$

$$\frac{\partial T}{\partial t} - v\frac{\partial T}{\partial z} + \boldsymbol{u} \cdot \nabla T = Le\nabla^2 T + F(c), \tag{2.2d}$$

with boundary conditions

$$\boldsymbol{u} \sim 0 \quad \text{as} \quad z \to \pm\infty, \tag{2.3a}$$

$$c, T \sim 0 \quad \text{as } z \to \infty, \tag{2.3b}$$

$$c, T \sim 1 \quad \text{as } z \to -\infty, \tag{2.3c}$$

with $\boldsymbol{e}_z$ being the unit vector pointing in the z-direction. For simplicity, we consider the simple cubic kinetic scheme $F(c) = c(1 - c)(c + d)$ with $d = 0.0021$ a typical experimental value for chemical fronts (Vasquez, Wilder & Edwards 1996; De Wit 2001, 2004). The Lewis number $Le = D_T/D_c$ with D_T being the medium thermal diffusivity. Equations (2.2) have been written in the Boussinesq approximation and all physical parameters of the fluid are assumed constant. This is justified as autocatalytic fronts typically imply relative solutal and thermal density jumps across the front that are of the order of 10^{-4} as the solutions are dilute and the temperature changes only of a few Kelvin. It should be noted that with $K = w^2/12$ these equations also model the flow in a Hele-Shaw cell of small gap width w. The thermal and solutal Rayleigh numbers are defined by

$$R_T = \frac{g\alpha_T K \Delta T}{\nu U}, \quad R_c = \frac{g\alpha_c K \Delta c}{\nu U} \tag{2.4}$$

where ν is the kinematic viscosity. Positive Rayleigh numbers imply static instability when the wave-front speed $v > 0$, i.e. for fronts ascending in the gravity field. Negative stabilizing Rayleigh numbers can result from the four different combinations of the signs of α_T and α_c (with $\Delta T < 0$ as appropriate for endothermic reactions), or front propagation in the direction of gravity and allow the study of the double-diffusive

phenomenon.† Consider now the two-dimensional transverse instability of the basic ascending reaction–diffusion front c_s, v, T_s. This base state is obtained as solution of equations (2.2) and (2.3) with $\boldsymbol{u}=0$ and takes the form

$$c_s(z)=\left\{1+\mathrm{e}^{z/\sqrt{2}}\right\}^{-1}, \quad v=\frac{1+2d}{\sqrt{2}}, T_s(z) \tag{2.5}$$

with $T_s(z)=c_s(z)$ for $Le=1$ and numerically determined for $Le>1$. We analyse the stability of this base state with regard to possible flows driven by density gradients as described by the system (2.2) and (2.3). Linear stability analysis leads to an eigenvalue problem for the perturbations $\{\overline{c},\overline{T},\overline{u}\}(z)\exp(\mathrm{i}ky+\sigma t)$ in respectively the concentration, temperature and vertical velocity (D'Hernoncourt *et al.* 2006):

$$\sigma\overline{c}-v\overline{c}'+c_s'\overline{u} = \overline{c}''-k^2\overline{c}+\frac{\mathrm{d}F}{\mathrm{d}c}\Big|_{c_s}\overline{c}, \tag{2.6a}$$

$$\sigma\overline{T}-v\overline{T}'+T_s'\overline{u} = Le(\overline{T}''-k^2\overline{T})+\frac{\mathrm{d}F}{\mathrm{d}c}\Big|_{c_s}\overline{c}, \tag{2.6b}$$

$$\overline{u}''-k^2\overline{u} = -k^2(R_T\overline{T}+R_c\overline{c}), \tag{2.6c}$$

$$\overline{c},\overline{T},\overline{u}\sim 0 \ \text{ as } \ z\to\pm\infty. \tag{2.6d}$$

Here k,σ are the wavenumber and growth rate of the perturbations, primes correspond to derivatives with respect to z and $\mathrm{d}F/\mathrm{d}c$ is evaluated at the base state (2.5). We solve (2.6) by both-second order finite differences and pseudospectral Chebyshev methods. For each R_T and Le, and for each k, R_c is calculated so that

$$\max(\mathrm{Re}\{\sigma(R_c,k,Le,R_T)\}=0. \tag{2.7}$$

The critical solutal Rayleigh number $R_{c_{cr}}$ and the critical wavenumber k_{cr} are determined by minimization over k. Long computational domains in the z-direction were required in order to accurately resolve the base state and the eigenfunctions, in particular at the largest values of Le computed here. A truncated infinity of $|z|\leqslant 300$ is found necessary with $Le=10$ and required about 300–500 spectral coefficients or 1000–2000 mesh points for each variable. For the finite differences method the size of the domain is taken up to 800 and the mesh size down to $\mathrm{d}z=0.25$.

3. Results

It is instructive to first recall the classical model of a horizontal layer of height h with the lower boundary maintained at $c^*+\Delta c$ and $T^*+\Delta T$ while the upper boundary is kept at c^* and T^* (Nield & Bejan 1992). With the scales $h, h^2/D_c$ and D_c/h for respectively length, time, and velocity, the linear stability problem is governed by (2.6) with $F=v=0$, $c_s=T_s=1-z$ and the boundary conditions imposed at $z=0$ and 1. The critical eigenfunction is $\sin(z\pi)$ and the dispersion relation is (Nield & Bejan 1992)

$$k^2+\pi^2=\frac{k^2R_T}{Le(k^2+\pi^2)+\sigma}+\frac{k^2R_c}{(k^2+\pi^2)+\sigma}, \tag{3.1a}$$

† Note that in D'Hernoncourt, Zebib & De Wit (2006), the negative sign present in the definition of the Rayleigh numbers (2.4) and of the density (3.4) is due to the consideration of a downward moving front while here we analyse an upward moving one to correspond to usual conventions used in the double-diffusive literature.

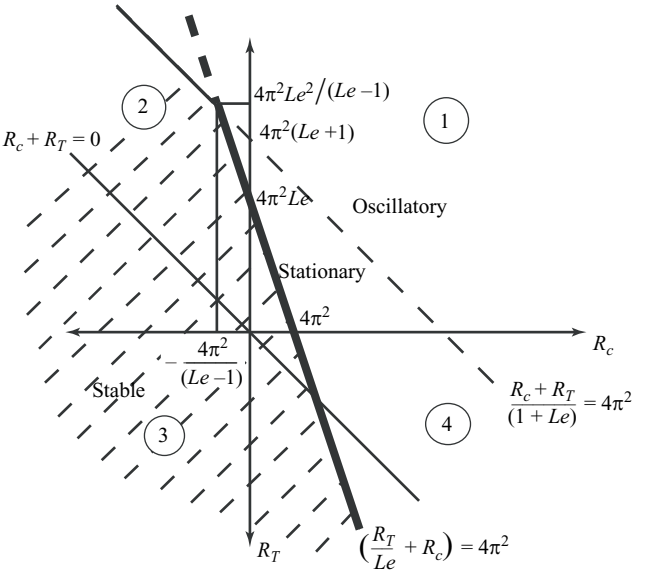

FIGURE 1. Classical hydrodynamic stability boundaries for a finite porous layer with $Le > 1$. The basic state is stably stratified below the line $R_T + R_c = 0$.

with

$$R_T = \frac{g\alpha_T K h \Delta T}{\nu D_c}, \quad R_c = \frac{g\alpha_c K h \Delta c}{\nu D_c}. \tag{3.1b}$$

Note that, contrary to the classical case, the thermal Rayleigh numbers in the definitions (2.4) and (3.1*b*) are here constructed using D_c instead of D_T. The stationary branch of the stability boundary is given by

$$k = \pi, \ \frac{R_T}{Le} + R_c = 4\pi^2 \tag{3.2}$$

which corresponds to the bold curve in figure 1. For $R_c = 0$, the threshold above which the Rayleigh–Bénard instability sets in is $R_T = 4\pi^2 Le$, i.e. it is an increasing function of Le. For $R_T = 0$, the corresponding solutal threshold is $R_c = 4\pi^2$. On the oscillatory branch obtained for $Le > 1$ we have

$$k = \pi, \ R_T + R_c = 4\pi^2(Le+1), \ -R_c > \frac{4\pi^2}{Le-1} \tag{3.3}$$

drawn as a thin (partly dashed) line on figure 1. The complete stability boundary corresponding to $Le > 1$ shown in figure 1 can be summarized as follows: it is observed that above the threshold values the flow is unstable to the direct mode in quadrant 1 ($R_c \geqslant 0$ and $R_T \geqslant 0$), and stable in quadrant 3 ($R_c \leqslant 0$ and $R_T \leqslant 0$). The direct double-diffusive regime operates in quadrant 4 ($R_c \geqslant 0$ and $R_T \leqslant 0$) and oscillatory double-diffusive modes act in quadrant 2 ($R_c \leqslant 0$ and $R_T \geqslant 0$).

We now turn to the analysis of the influence of chemical reactions on this stability diagram by focusing on the case of the chemical front. Stationary stability boundaries for $Le = 1$, 3 and 10 are shown in figure 2. With $Le = 1$, $T_s = c_s$ as given in (2.5) and the stability boundary is simply the straight line $R_T = -R_c$. This is easily understood by inspecting the basic dimensionless density profile

$$\rho = -R_T T - R_c c \tag{3.4}$$

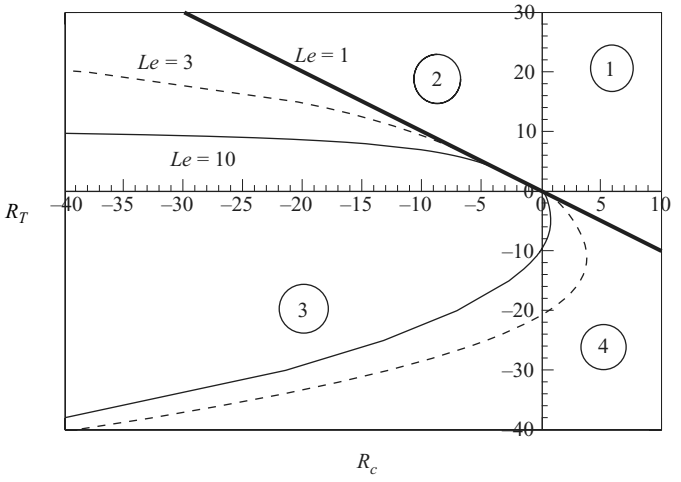

FIGURE 2. Stability boundaries for the case of a chemical front. For $Le = 1$, the system is stable below the bold line $R_T = -R_c$. For $Le = 3$ and 10, the stability domain is the tongue delineated by the dashed and full lines respectively. In particular, the flow is unstable when $R_c = 0$ and $R_T < R_1 = -20.67$ ($Le = 3$), and $R_c = 0$ and $R_T < R_1 = -9.51$ ($Le = 10$).

where $\rho = (gK/\nu u)(\rho^*/\rho_0)$. The basic density profile gradient is

$$\frac{\mathrm{d}\rho_s}{\mathrm{d}z} = -R_T \frac{\mathrm{d}T_s}{\mathrm{d}z} - R_c \frac{\mathrm{d}c_s}{\mathrm{d}z} \tag{3.5}$$

which, for $Le = 1$ and using (2.5), gives

$$\frac{\mathrm{d}\rho_s}{\mathrm{d}z} = \frac{R_T + R_c}{\sqrt{2}} \frac{\mathrm{e}^{z/\sqrt{2}}}{\left(1 + \mathrm{e}^{z/\sqrt{2}}\right)^2}. \tag{3.6}$$

This vertical gradient of the basic density is positive above the line $R_T = -R_c$ for an ascending front and is thus unstably stratified with regard to buoyancy. The sharp interface created by the chemical front between the products and reactants triggers the instability as soon as $R_T + R_c > 0$ and thus the instability threshold observed in quadrant 1 of figure 1 is no longer present. This is the first important difference between the reactive and non-reactive cases.

With $Le > 1$ the flow is unstable above the upper branches $R_c \leqslant 0$ and $R_T > R_{T_{cr}} > 0$ of quadrant 2, below the lower branches $R_c \leqslant 0$ and $R_T < R_{T_{cr}} < 0$ of quadrant 3, and in almost all of quadrant 4 except where it is stable in the small region bounded by $R_T \leqslant R_1(Le) < 0$ and $R_c < R_{c_{cr}} > 0$. It is thus seen that the region of stability has shrunk considerably and continues to get smaller as Le increases, in sharp contrast to the classical case in figure 1.

Consider first the chemically driven instability at the lower branches in quadrant 3 with $R_c \leqslant 0$ and $R_T < R_{T_{cr}} < 0$ shown in figure 2. Here both R_T and $R_c < 0$ so that according to (3.5), $\mathrm{d}\rho_s/\mathrm{d}z < 0$ throughout the field as T_s and c_s are decreasing functions of z and stability is expected. A physical explanation of this light-over-heavy gravitational instability emerges from an examination of the basic profiles in figure 3 with $Le = 10$ in the region where $F(z)$ increases as a particle is displaced upward. Because $Le > 1$ slower species diffusion allows the displaced particle to maintain its concentration. Thus both the energy and concentration chemical sources associated with the displaced particle are smaller than those of the surroundings

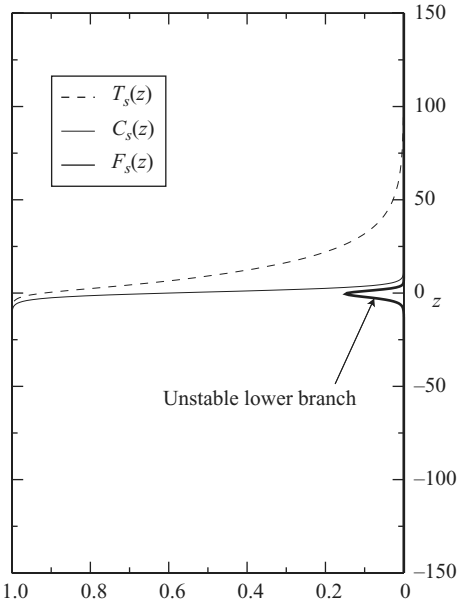

FIGURE 3. The basic profiles c_s, T_s and F_s driving the new instability ($Le = 10$). Our physical argument predicts local instability of a stably stratified upward moving front with $R_T < 0$ and $R_c \leqslant 0$ in the area where $\mathrm{d}F/\mathrm{d}z > 0$.

(because $\mathrm{d}F/\mathrm{d}z > 0$), hence it can be at a lower temperature and concentration. Since (3.4) in this case becomes

$$\rho = |R_T|T + |R_c|c, \tag{3.7}$$

the particle displaced upward can be lighter than its neighbours; it may continue to rise. This chemically driven mechanism of instability is operative only in the region where $\mathrm{d}F/\mathrm{d}z > 0$. In the zone where the gradient has opposite sign, i.e. where $\mathrm{d}F/\mathrm{d}z < 0$, the displacement argument explained above leads to stability. Indeed, in that case, the reaction is more active inside the particle displaced upwards which thus becomes hotter and more concentrated in products (larger T and c). According to (3.7), the particle is then heavier than its surroundings and comes back to its initial position. Hence, as the unstable region with $\mathrm{d}F/\mathrm{d}z > 0$ lies below a region with $\mathrm{d}F/\mathrm{d}z < 0$, it follows that a region of local chemical stability supercedes the region of local instability. This is also revealed by the critical eigenfunctions shown in figure 4 (with the infinity norm = 1) where the disturbances are largest below the advancing chemical front centred at $z = 0$ and moving in the direction of positive z. Note that this new instability mode is magnified at larger $|R_T|$ since according to (3.7) small changes in T are more effective in changing the density at larger $|R_T|$, and at larger $Le > 1$ because slower mass diffusion results in a larger difference in the chemical sources associated with the displaced particle and its new environment. This is clearly supported by the linear stability calculations in figure 2. In figure 4, we also plot the value of the most unstable wavenumber k_{max} along with the corresponding maximum growth rate σ_{max}. For a fixed R_c, the growth rate and the corresponding wavenumber are increasing when R_T is decreased below R_{Tcr}, confirming that the system becomes more unstable with decreasing R_T. The threshold R_{Tcr} is also decreased with decreasing $R_c < 0$: in this case, static stability increases

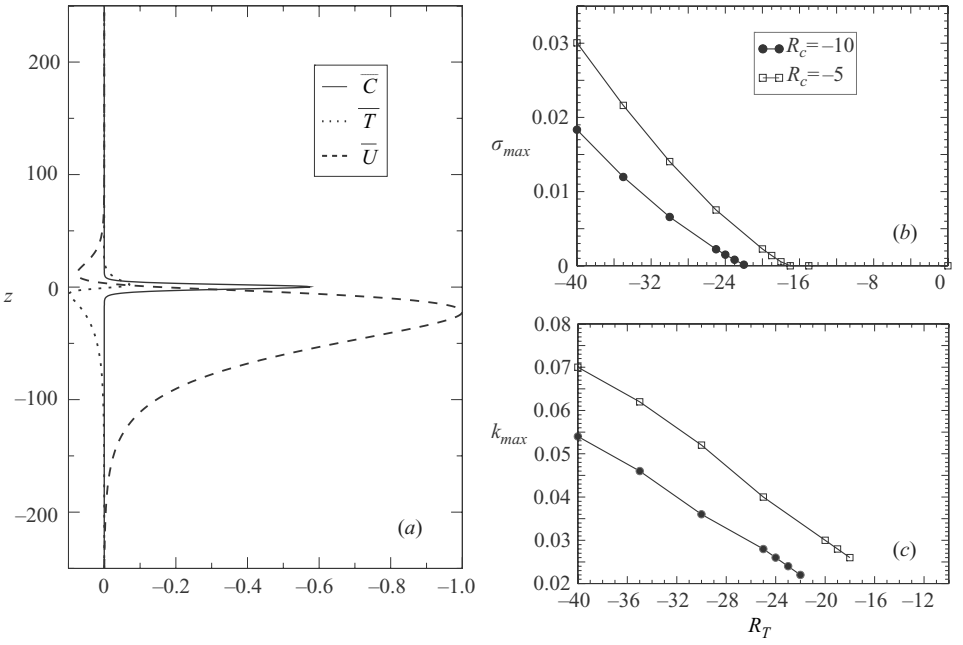

FIGURE 4. (*a*) Most unstable linear eigenfunction with $R_c = -5$, $R_T = -30$ ($Le = 10$). The perturbation is largest below the front in the zone where $\mathrm{d}F/\mathrm{d}z > 0$. (*b*) Variations of maximum growth rate and (*c*) corresponding wavenumber with R_T at two fixed values of R_c.

and the magnitude of $R_T < 0$ necessary to drive instability must increase to overcome the additional static stability imposed by $R_c < 0$.

Quadrant 3 is thus characterized by a chemically driven instability of a solute-poor and hot fluid overlying a solute-rich and cold one. Quadrants 2 and 4 are also clearly affected by the chemical reactions. A close examination of eigenfunctions as well as the most unstable growth rates and wavenumber shows that in these quadrants, the stability domain results from a mixture of the chemically driven mechanism explained above and of local unstable Rayleigh–Taylor zones.

Let us first examine quadrant 2 where the solutal effect is stabilizing ($R_c < 0$) while the thermal one is destabilizing ($R_T > 0$). When $Le > 1$, the thermal front is more spread out than the concentration front and the system therefore exhibits localized zones of static Rayleigh–Taylor thermally driven instability with $\mathrm{d}\rho_s/\mathrm{d}z > 0$ ahead of the front, as shown in figure 5 where we plot $\rho_s(z)$ and the eigenfunctions on the same graphs.

In addition the chemical mechanism drives an unstable region behind the front. Again because $Le > 1$, slower species diffusion allows the particle displaced upward in the zone where $\mathrm{d}F/\mathrm{d}z > 0$ to maintain its concentration while quickly reaching the same temperature as the environment. The chemical source associated with the displaced particle is smaller than that of the surroundings, hence it can evolve to a lower temperature and concentration than the surroundings and continue to rise. Since in this case

$$\rho = -R_T T + |R_c| c \tag{3.8}$$

there is a competition between R_T and R_c with a lighter displaced particle resulting owing to both the larger $|R_c|$ and the faster tendency to thermal equilibrium with

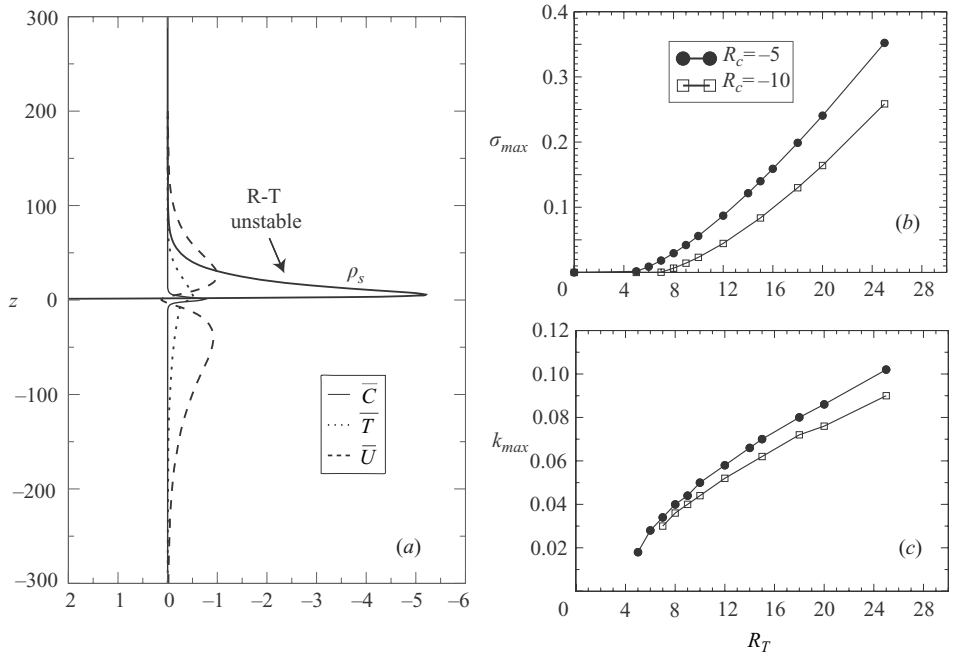

FIGURE 5. Similar to figure 4 with (a) most unstable linear eigenfunction along with the basic density profile $\rho_s(z)$ for the critical point in quadrant 2 where $R_c = -33.3$ and $R_T = 9.5$ ($Le = 10$). The large positive value of ρ_s for $z < 0$ is not shown here on this scale. The locally unstable density stratification ahead of the front drives locally a Rayleigh–Taylor (R-T) instability while the chemical mechanism operates below the front.

$Le > 1$. This scenario is also confirmed by the eigenfunctions in figure 5 where the disturbance is seen to take place both behind and ahead of the advancing front. Here however the instability is not inhibited by an overlying stable region. This probably explains the very small increase in the magnitude of $R_{T_{cr}}$ associated with the upper branch, with decrease in $-R_c$, compared with the lower branch. Figure 5 also shows that the growth rate and wavenumber of the most unstable mode increase monotonically with increasing R_T for a fixed R_c. Equation (3.8) suggests potential overstability, e.g. the oscillatory branch exhibited in figure 1. While oscillatory modes do exist we could not find any critical overstable states.

Let us now focus on quadrant 4 which features a complex mixture of instabilities due to Rayleigh–Taylor and chemically driven mechanisms. Here solutal effects are destabilizing ($R_c > 0$) while heat effects are stabilizing ($R_T < 0$). For $Le > 1$, we observe in figure 6 that the density profile features a localized zone where $\mathrm{d}\rho_s/\mathrm{d}z > 0$ which is thus susceptible to a Rayleigh–Taylor instability. For a given R_c this mechanism disappears when R_T is decreased, i.e. when stabilizing thermal effects become dominant. In non-reactive fluids, it is known that the system becomes stable below a given critical R_T for each R_c. This is not what is observed in the reactive case however because when $|R_T|$ is large enough the chemically driven mechanism takes over. Consider first the small value $R_c = 0.2$. A close inspection of the most unstable wavenumber and growth rate shows that the system is stable for $-8.8 < R_T < -0.43$. This means that the solutal effect is mostly too weak to destabilize the system and that the chemically driven effect becomes operative only for strong enough thermal effects. If R_c is larger, i.e. for $R_c = 1$ as shown in figure 6, the system becomes

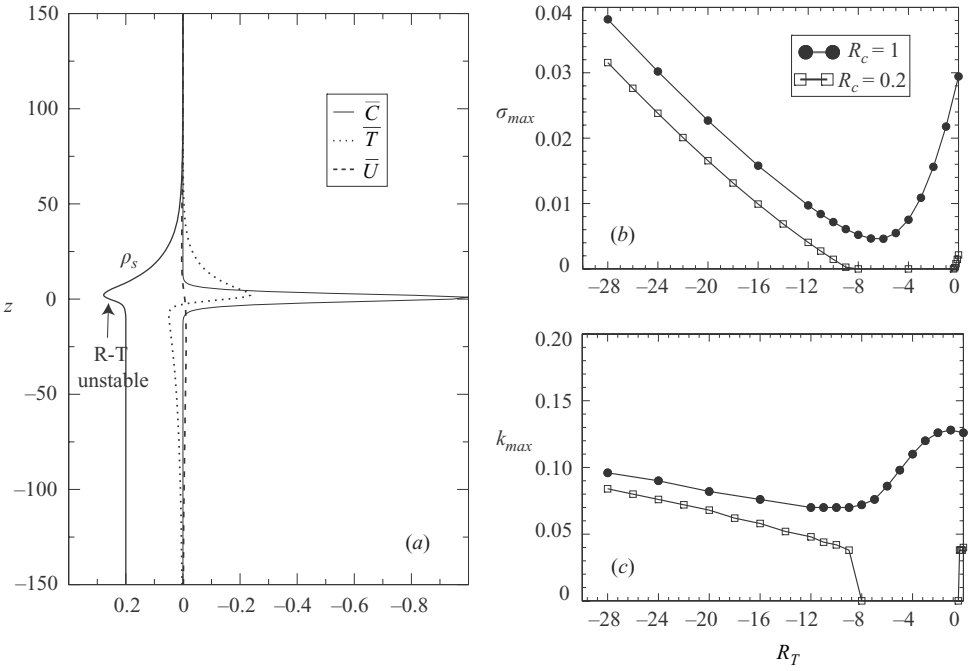

FIGURE 6. Similar to figure 4 with (*a*) most unstable linear eigenfunction along with the basic density profile $\rho_s(z)$ for the critical point in quadrant 4 where $R_c = 0.2$ and $R_T = -0.4$ ($Le = 10$). The locally unstable density stratification centred around $z = 0$ drives a Rayleigh–Taylor (R–T) instability both below and ahead of the front while the chemical mechanism operates below the front.

immediately unstable due to the solutal Rayleigh–Taylor mechanism, even when R_T is decreased. This effect weakens when R_T decreases, thus increasing static stability, until the chemically driven effect magnifying when R_T decreases takes over. This results in a non-monotonic change in σ_{max} and k_{max} with decreasing R_T (see figure 6).

The stability behaviour in the presence of chemical reactions thus changes drastically in all four quadrants.

4. Conclusions

We have analysed a reaction–diffusion–convection model describing convective instabilities generated in porous media by concentration and temperature gradients either imposed across a layer of non-reactive fluids or generated dynamically by a chemical reaction inside a chemical front. Using a linear stability analysis, we have compared the stability domains of both cases in the parameter space spanned by the thermal R_T and solutal R_c Rayleigh numbers to gain insight into the influence of chemical reactions on buoyancy-driven instabilities. We find that chemistry has a significant influence as the region of stability of chemical fronts is much smaller than its classical hydrodynamic counterpart. The stability region further diminishes with increasing Le in marked contrast to the classical case.

First, the first quadrant, in which $R_T \geqslant 0$ and $R_c \geqslant 0$, is entirely unstable in the case of chemical fronts. There are no threshold critical values for the Rayleigh numbers as in the classical hydrodynamic Rayleigh–Bénard type of instability across a fluid layer in which an adverse imposed linear gradient of temperature or mass must be

strong enough to overcome stabilizing viscous effects. In the case of chemical fronts in quadrant 1, the transition zone between the heavy reactants at room temperature and the hot and light products is so small that we basically have to consider the Rayleigh–Bénard and Rayleigh–Taylor instabilities between two semi-infinite regions with the heavy fluid on top of the light one-which is then always unstable.

In addition, three other branches of the stability boundary exist in the (R_T, R_c)-plane. The main difference between the classical and reactive cases exists in quadrant 3 where solutal and thermal effects both contribute to a stable density stratification with R_T and R_c both negative. In non-reactive systems, that quadrant is always absolutely stable. On the contrary, in the presence of a chemical reaction, buoyancy-driven instabilities of globally statically stable propagating reaction–diffusion fronts have been identified. Displaced-particle arguments reveal the roles played by chemistry and double diffusion in driving the convection.

The branch in quadrant 2 corresponds to an upward propagating front with $R_T \geqslant 0$ and $R_c \leqslant 0$. Instability is driven behind the front by chemistry and ahead of the front as a local Rayleigh–Taylor instability. It is somewhat surprising that the classical oscillatory diffusive branch has disappeared in the linear analysis. While complex eigenvalues are present in the spectrum they never dominate. Oscillatory states should be pursued in nonlinear studies. The third branch in quadrant 4 ($R_T \leqslant 0$ and $R_c \geqslant 0$) where traditional direct double-diffusive modes exist is driven by the same chemical mechanism as quadrant 3 behind the front, in addition to a locally unstable stratification that straddles the front. Thus almost all of quadrant 4 is unstable.

We have thus shown that chemical reactions drastically change the stability properties of fluids with regard to buoyancy-driven instabilities. Most importantly, we have shown that the general intuition that hydrodynamicists have in mind when considering a stability plane such as in figure 2 cannot be used if chemical reactions are at play. Our work should therefore be the starting point of further examinations of the role played by chemistry in several applications where buoyancy-driven instabilities are important. First, it would be useful to analyse in detail to what extent our conclusions carry over to combustion in porous media. All the elements necessary for the chemically driven instability to operate, i.e. a localized reaction zone and differential diffusivity of heat and mass, are present. However, in addition, a theoretical study of the influence of an Arrhenius law and of the validity of the Boussinesq approximation should be conducted. In the same spirit, it would be interesting to test the robustness of our findings with regard to the type of kinetics used in other applications. These include convective instabilities in bio-remediation or reactive geological flows in porous media for instance. Further studies should also generalize our results to the case of flows in non-porous media using the full Navier–Stokes equations.

It should be pointed out that an upward propagating autocatalytic front with a positive Rayleigh number is identical to a downward propagating front with a negative Rayleigh number of the same magnitude (D'Hernoncourt *et al.* 2006). Thus our theory is easily amenable to experimental verification in an experimental set-up based on a Hele-Shaw geometry in the wide class of existing autocatalytic chemical fronts.

J. D. is supported by a FRIA (Belgium) PhD fellowship. A. D. acknowledges financial support of Prodex (Belgium), ESA, FNRS and of the Communauté française de Belgique ("Actions de Recherches Concertées" programme). A. Zebib acknowledges

the Donors of the American Chemical Society Petroleum Research Fund for support of this research.

REFERENCES

Baines, P. G. & Gill, A. E. 1969 On thermohaline convection with linear gradient. *J. Fluid Mech.* **37**, 289–306.

De Wit, A. 2001 Fingering of chemical fronts in porous media. *Phys. Rev. Lett.* **87**, 054502.

De Wit, A. 2004 Miscible density fingering of chemical fronts in porous media: Nonlinear simulations. *Phys. Fluids* **16**, 163–175.

D'Hernoncourt, J., Zebib, A. & De Wit, A. 2006 Reaction driven convection around a stably stratified chemical front. *Phys. Rev. Lett.* **96**, 154501.

Kalliadasis, S., Yang, J. & De Wit, A. 2004 Fingering instabilities of exothermic reaction–diffusion fronts in porous media. *Phys. Fluids* **16**, 1395–1409.

Khan, A. A. & Zebib, A. 1981 Double diffusive instability in a vertical layer of a porous medium. *J. Heat Transfer* **103**, 179–181.

Nield, D. A. 1968 Onset of thermohaline convection in porous media. *Water Resour. Res.* **11**, 553–560.

Nield, D. A. & Bejan, A. 1992 *Convection in Porous Media.* Springer.

Pojman, J. A. & Epstein, I. R. 1990 Convective effects on chemical waves. 1. Mechanisms and stability criteria. *J. Phys. Chem.* **94**, 4966–4972.

Pojman, J. A. & Epstein, I. R. 1998 *An Introduction to Nonlinear Chemical Dynamics.* Oxford University Press.

Turner, J. S. 1973 *Buoyancy Effects in Fluids.* Cambridge University Press.

Vasquez, D. A., Wilder, J. W. & Edwards, B. F. 1996 Chemical wave propagation in Hele-Shaw cells and porous media. *J. Chem. Phys.* **104**, 9926.